Magnetic phase transition in Fe-doped topological insulator Bi_2Se_3

Jeongwoo Kim[1,2] and Seung-Hoon Jhi[1,*]

[1]*Department of Physics, Pohang University of Science and Technology, Pohang 790-784, Republic of Korea*

[2]*Department of Physics and Astronomy, University of California at Irvine, Irvine, California 92697, USA*

(Received 23 July 2014; published 8 September 2015)

We study the effect of Fe impurities in Bi_2Se_3 on the magnetic phase and topological insulating property using first-principles calculations. In particular, we investigate the ferromagnetic-antiferromagnetic phase transition and the energy gap variation of surface states in Fe-doped Bi_2Se_3. We find that Fe-doped Bi_2Se_3 has a ferromagnetic phase at dilute doping regime by the interplay of the band inversion and intrinsic doping. For higher Fe concentration, >1.7 at. %, Bi_2Se_3 prefers the antiferromagnetic phase mediated by the superexchange interaction. We show that neighboring Fe impurities with antiferromagnetic ordering behave like nonmagnetic scattering centers that preserve the linear band dispersion and the in-plane spin texture of topological surface states. Our result indicates that interdependency of the magnetic phase and the band topology in transition-metal–doped topological insulators may tweak the electronic structure and topological surface states in peculiar ways.

DOI: 10.1103/PhysRevB.92.104405 PACS number(s): 75.50.Pp, 71.15.Mb, 73.20.At

I. INTRODUCTION

Topological insulator (TI) is a new quantum state of matters characterized by insulating bulk and metallic surface electronic structures [1–4]. When the spin-orbit coupling (SOC) exceeds the band gap to induce the band inversion, nontrivial band topology may arise, and consequently, helical conducting states form at the surfaces with robustness against defects as enforced by the time-reversal symmetry (TRS) [5,6]. Manipulation of this topological surface state (TSS) is considered as an essential step for exploring exotic phenomena and for application as well [7–9]. In particular, breaking TRS and subsequent gap opening by transition-metal doping in topological insulators is of great interest as a way to realize the quantum anomalous Hall effect [10,11].

Transition metals are expected to induce TRS breaking in TI and to destroy the linear band dispersion and helical spin structure of TSS. There have been controversies over the presence of gap openings upon transition-metal doping in TI. For instance, a clear signature of gap opening is missing in experiments of Fe adsorption on TI surfaces [12,13], while the gap opening was reported in Fe-doped TIs [14,15]. Another intriguing finding in the latter case is the band-gap size of TSS in Fe-doped TIs that decreases at high Fe concentrations [15]. Also Fe-doped TIs exhibit interesting magnetic phase transitions from ferromagnetic (FM) to antiferromagnetic (AFM) phase as the Fe doping ratio exceeds the critical concentration of about 1.5 at. % [15]. It is very unusual that the magnetic phase transition occurs without pressure or temperature control in dilute magnetic semiconductors. The trend in the energy gap of TSS and the magnetic phase transition upon Fe doping indicate that the band topology and magnetic phases in transition-metal–doped TIs may be interconnected in a more complex way than anticipated, opening the possibility of tweaking electronic structures while preserving the exotic surface states.

In this work we study the magnetic ordering and its transition and the behavior of TSS in Fe-doped TIs using first-principles calculations. We investigate the ground magnetic phase of Fe-doped Bi_2Se_3 and the mechanism of magnetic ordering upon varying Fe concentrations. We also investigate the effect of magnetic defects on TSS with changing the position and magnetic ordering of Fe impurities.

II. METHOD

Calculations are performed using the first-principles self-consistent pseudopotential method [16] as implemented in the Vienna *ab initio* simulation package (VASP) [17]. The exchange correlation of electrons is approximated as the generalized gradient approximation (GGA) in the form of Perdew-Burke-Ernzerhof [18]. SOC is included in the self-consistent calculations. The cut-off energy for the plane-wave–basis expansion is chosen to be 300 eV. We employ a $3 \times 3 \times 2$ k-point grid for the bulk system with a variation in the number of atoms from 135 to 270 and a $3 \times 3 \times 1$ k-point grid for the slab structure containing 225 atoms. To describe the long-range dispersion interaction properly, we employed the van der Waals correction suggested by Tkatchenko and Scheffler as implemented in VASP [19].

III. RESULTS AND DISCUSSION

We considered substitutional Fe defects at Bi sites which are energetically more favorable than other sites [20]. First we studied the change in the topological phase of Bi_2Se_3 due to the magnetic impurities in the dilute doping regime of about 1%. Figure 1 shows calculated band structures. Without Fe doping [Figs. 1(a) and 1(c)], we observe a shift of the valence band in the Γ-M direction toward the Fermi level and the anticrossing at Γ point by the SOC, which indicates a change in the band topology [21]. Upon Fe doping to Bi_2Se_3, we observe the appearance of Fe d bands and a reduction in the band gap from hybridization of TI and Fe [Figs. 1(b) and 1(d)]. Our calculations show that Fe impurities have a high spin configuration with a net magnetic moment of $5\,\mu_B$ as the exchange energy surpasses the crystal splitting under octahedral symmetry. In order to check the tendency of Fe aggregation in Bi_2Se_3, we calculated the total energy of Fe-doped Bi_2Se_3 for varying inter-Fe distance. Our

*Corresponding author: jhish@postech.ac.kr

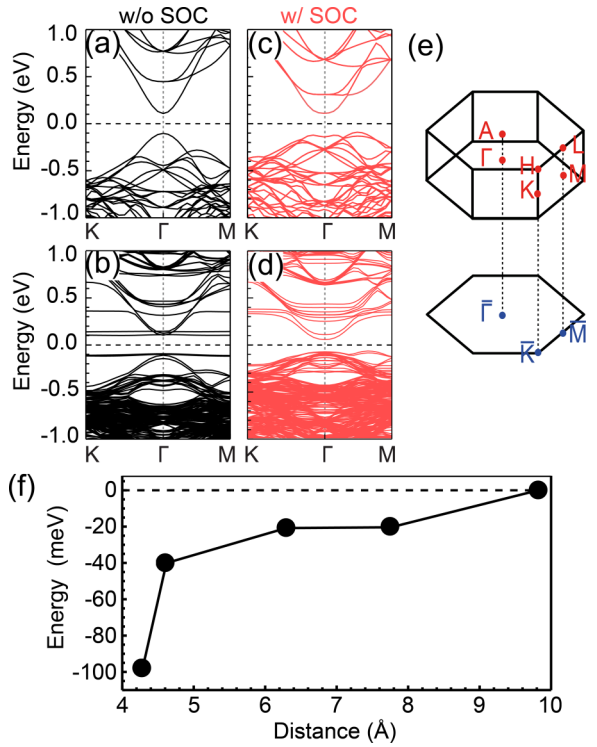

FIG. 1. (Color online) (a)–(d) Calculated band structures of (a,c) pristine and (b,d) Fe-doped (1 at. %) Bi_2Se_3; calculations (a, b) without and (c, d) with SOC. The Fermi level is denoted by the dashed line at zero energy. (e) The first Brillouin zone for the bulk and the surface projection with the special k points. (f) Calculated total energy for varying Fe distance relative to the case of a dilute regime (Fe distance of 10 Å).

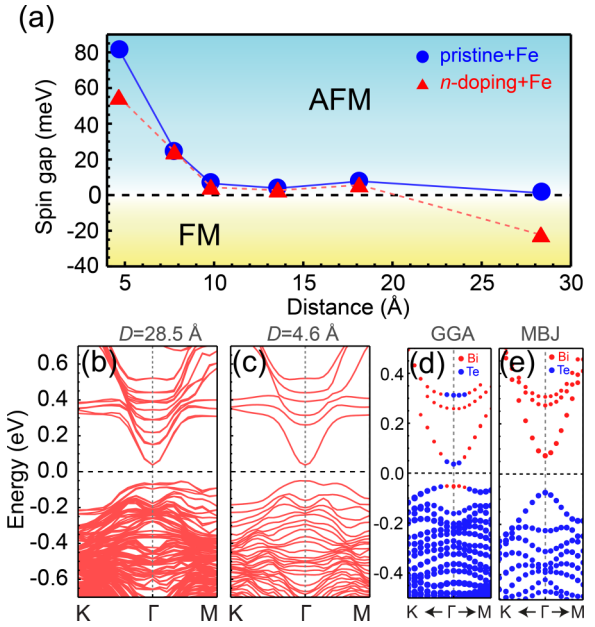

FIG. 2. (Color online) (a) Calculated spin gap (the energy difference between FM and AFM phase) as a function of inter-Fe distance (D); positive (negative) if AFM (FM) phase is the ground magnetic state. Blue dots (red triangles) for Fe-doped Bi_2Se_3 without (with) n doping. (b, c) Calculated band structure of Fe-doped Bi_2Se_3 with inter-Fe distance of 28.5 and 4.6 Å, respectively. (d, e) The states near the Fermi level for Fe distance of 4.6 Å calculated with the GGA and MBJ potentials, respectively. Red (Blue) dots denote Bi (Te) atomic character.

calculations in Fig. 1(f) indicate that Fe may cluster instead of dispersing randomly.

Next we studied the ground magnetic phase of Fe-doped Bi_2Se_3 with variation in inter-Fe distance from 4.6 to 28.5 Å. The calculated spin gap (the energy difference between FM and AFM states) in Fig. 2(a) shows that the AFM state is favored, regardless of Fe interatomic distance in the pristine case [20]. The effect of the magnetic exchange responsible for AFM ordering disappears quickly when the interatomic distance exceeds 10 Å. A primary mechanism of AFM ordering in Bi_2Se_3 is the superexchange interaction, which is the second-order hopping process mediated by anions [22,23]. Electronic structures of Bi_2Se_3 with Fe impurities in AFM ordering are almost the same, irrespective of inter-Fe distance [Figs. 2(b) and 2(c)].

We also studied the effect of intrinsic doping on the magnetic phase of Fe-doped Bi_2Se_3. Chalcogenide TIs such as Bi_2Se_3 and Bi_2Te_3 usually have bulk conduction due to anionic vacancy defects [24,25], and external doping is thus required to obtain the insulating property. We emulated the n-type doping observed in experiment by shifting the Fermi level [15]. The calculated spin gap for n-type doping of 2.6×10^{-4} e/Å^3 that corresponds to a Fermi level shift of 0.25 eV is also plotted in Fig. 2(a). The AFM ordering is stable for an Fe interatomic distance of 20.5 Å or shorter, but the FM ordering becomes the ground phase when Fe interatomic distance exceeds 20.5 Å. The inter-Fe distance of ∼20.5 Å corresponds to an Fe concentration of about ∼1.7 at. % at uniform dispersion, which is similar to the experimental value [15]. The Curie and Néel temperatures of Fe-doped Bi_2Se_3 are estimated under the mean-field approximation to be about 50 K for the ferromagnetic phase at a dilute Fe doping regime (about ∼0.63 at. %) and less than ∼10 K for the antiferromagnetic phase (at a moderate Fe doping condition <10 at. %). Here we set the spin gap to the coupling constant $2J$ in the Heisenberg model.

By increasing the n-doping level by shifting up the Fermi level, the metallicity of Fe-doped Bi_2Se_3 is enhanced and the long-range Ruderman-Kittel-Kasuya-Yosida (RKKY) type interaction between the TI conduction bands and localized Fe d orbitals becomes significant. In this case, the band inversion of TIs is essential for the FM phase to develop by the RKKY interaction. In conventional narrow-gap semiconductors, localized states of magnetic impurities are coupled to the valence electrons, known as hole-meditated RKKY interaction [26,27]. For TIs, the conduction-band edge has the same orbital character as the valence band has before the band inversion, and the conduction bands now work as mediating channels for the magnetic impurities. When the SOC is turned off in our calculations of Fe-doped Bi_2Se_3 with inter-Fe distance of ∼28.5 Å, the spin gap is very small, about −0.2 meV compared to −24 meV with the SOC. In this case, localized Fe atoms have independent paramagnetic states without any preferential spin direction, because the conduction bands without the band inversion cannot work as mediating channels for magnetic interactions. Fe-doped Bi_2Se_3 has the

FM ordering for Fe concentration <1.7% by the RKKY-type interaction, which is now allowed by the topological insulating property of Bi_2Se_3. For higher Fe concentration >1.7%, Fe atoms tend to aggregate, preferring AFM ordering mediated by the superexchange interaction. One caveat is that the band inversion in Fe-doped Bi_2Se_3 should be carefully checked because the band gap in first-principles calculations may not be properly produced, depending on the type of the exchange-correlation functionals. For example, the electronic structure calculated within the GGA for 3.7 at. % Fe doping has the band inversion (or the negative band gap), but it has no band inversion (the positive band gap) with the modified Becke-Johnson (MBJ) exchange potential [Figs. 2(d) and 2(e)] [28,29]. The topological insulating property of Bi_2Se_3, sustained at a dilute regime of Fe doping, may be broken as Fe doping level increases. The critical Fe doping level for the TI property to disappear is material dependent. For example, Bi_2Te_3 is more resistive to Fe doping than Bi_2Se_3, remaining in the TI phase for ~3.7 at. % in our calculations with the hybrid exchange-correlation functional.

One puzzling issue in experiment is the effect of Fe impurities on the surface states, which apparently shows different behavior depending on the position of Fe impurities [12–15]. We studied the TSS upon varying the position of Fe impurities. The calculated formation energy of Fe-doped Bi_2Se_3 in a slab structure [20],

$$\Delta H_f = E_{Fe+BS} - (E_{Vac+BS} + \mu_{Fe}),$$

where E_{Fe+BS} (E_{Vac+BS}) is the total energy of Bi_2Se_3 with an Fe impurity (a single vacancy) and μ_{Fe} is the chemical potential per atom of ferromagnetic bcc Fe, shows that Fe doping of 1% can be energetically stabilized regardless of Fe positions and that Fe impurities prefer the inner layers [Fig. 3(a)]. The energy gap is opened by the magnetic moment of Fe impurities, and its size depends on the position of Fe [Fig. 3(b)], reaching the maximum for Fe at the outermost quintuple layer and steadily decreasing for Fe moving into inner layers. Such dependence of the energy gap is due to strong hybridization between Fe impurities and topological surface states. For nonmagnetic impurities such as arsenic, we do not observe any gap opening in the surface states (with As at $Z = 5.52$ Å) [Fig. 3(c)]. This supports that the gap opening is due to the TRS breaking by magnetic impurities.

Next we investigated the effect of Fe clusters and their magnetic ordering on TSS. Our calculations show that Fe in Bi_2Se_3 prefers aggregation to dispersion. We consider an Fe impurity concentration of 4.4% with two Fe atoms at the nearest-neighboring Bi sites. It was found that the AFM ordering in the spins of an Fe dimer is more stable by 0.4 eV than the FM ordering and that the AFM ordering originates from the superexchange interaction. Fe-doped Bi_2Se_3 has an energy gap of ~50 meV for a single atomic Fe [Fig. 4(a)] but recovers the Dirac cone with clear in-plane spin helicity when Fe defects form dimers with antiparallel spin configuration (AFM ordering) [Figs. 4(b) and 4(e)]. The surface states reopen the gap if Fe dimers are forced to have less stable FM ordering [Fig. 4(c)]. As Fe-Fe distance of the dimers is increased, the AFM ordering is still preferred but a gap opens in the TSS [Fig. 4(d)]. This implies that the spin ordering in Fe dimers is closely related to the mass gap in the Dirac cone.

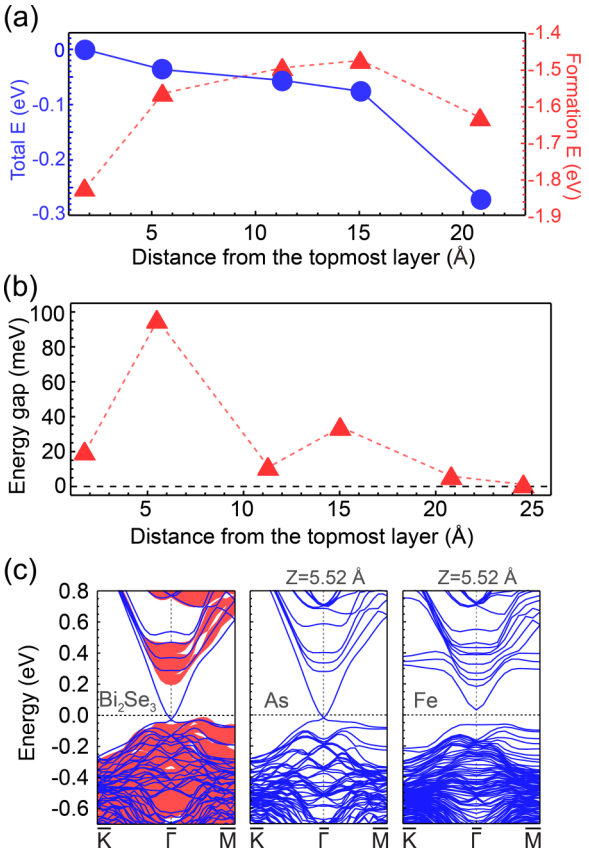

FIG. 3. (Color online) (a) Calculated total and formation energies of Fe-doped Bi_2Se_3 for varying Fe positions from the top layer. The energy reference is the value for Fe at the topmost layer. Fe impurities prefer the inner layers in Bi_2Se_3. (b) Calculated energy gap of TSS for varying Fe position from the surface. The gap is the maximum when Fe impurities are located at the TSS-localized layer. (c) From the left to right panels, calculated band structures of Bi_2Se_3 slab structure without defects, with arsenic doping, and with Fe doping. Z is the distance of the impurity from the topmost Se layer. The shaded region denotes the bulk band projection into the surface Brillouin zone.

In order to analyze this feature straightforwardly, we build a tight-binding Hamiltonian,

$$H = \sum_{\vec{k}\alpha\beta} \hbar v \vec{k} \cdot \vec{\sigma}_{\alpha\beta} c^{\dagger}_{\vec{k}\alpha} c_{\vec{k}\beta} + \sum_{i\tau\alpha} \varepsilon_{\tau} d^{\dagger}_{i\tau\alpha} d_{i\tau\alpha} + \sum_{\vec{k}i\tau\alpha\tau} V(d^{\dagger}_{i\tau\alpha} c_{\vec{k}\alpha} + \text{H.c.}) + \lambda_{so} \sum_{\tau,\tau',\alpha,\beta} d^{\dagger}_{i\tau\alpha} l_{\tau\tau'} \vec{\sigma}_{\alpha\beta} d_{i\tau'\beta},$$

where $c_{\vec{k}\alpha}$ and $d_{i\alpha\tau}$ are the operators for the surface Dirac fermion and Fe d electrons, respectively; α,β, the spin indices; i, site index of Fe; τ, d-orbital index; l, orbital angular momentum of the d orbital; and ε_{τ}, the on-site energy of d orbitals. $\vec{\sigma}$ denotes the Pauli matrices and v is the Fermi velocity. Here, V represents the hybridization of Dirac fermions with magnetic impurities and λ_{so} is the SOC strength. The parameters in the Hamiltonian were chosen by comparing the energy bands [Figs. 4(f) and 4(g)] to first-principles calculations; $V = 0.06$ eV, $\lambda_{so} = 0.03$ eV, and $\varepsilon_{\tau} = \pm 0.3$ eV. The surface states (the first term) are given

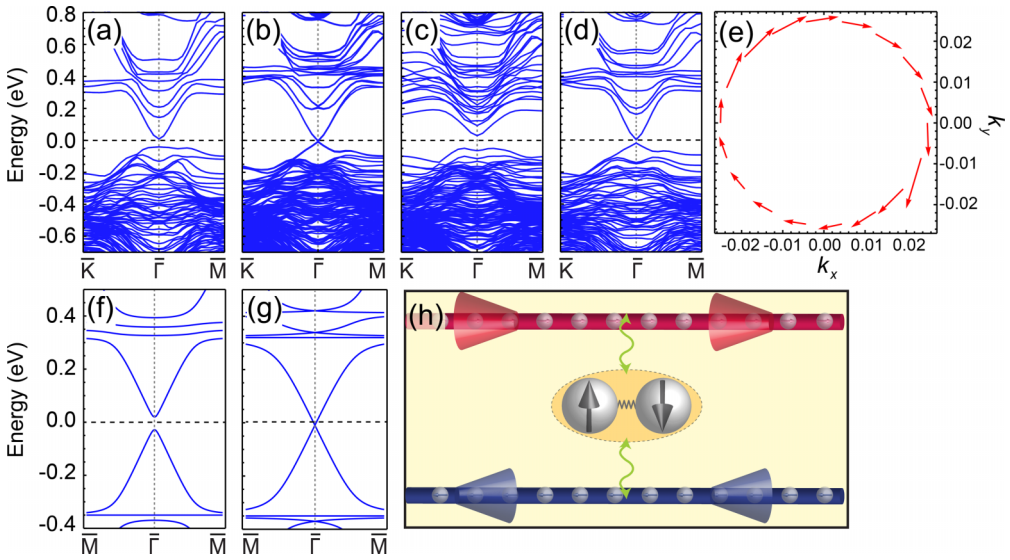

FIG. 4. (Color online) Band structures of Bi_2Se_3 slab calculated with first-principles method for (a) a single atomic Fe defect, (b) AFM- and (c) FM-ordered Fe dimers with inter-Fe distance of 4.11 Å, and (d) AFM-ordered Fe dimers with inter-Fe distance of 9.16 Å. (e) In-plane spin texture of the upper Dirac cone in (b). (f, g) Band structures of the tight-binding Hamiltonian for a single atomic Fe defect and AFM Fe dimers, respectively. The parameters chosen from the first-principles results are $V = 0.06\,\text{eV}$, $\lambda_{so} = 0.03\,\text{eV}$, and $\varepsilon_\tau = \pm 0.3\,\text{eV}$. (h) Schematics of TSS (blue and red arrows) interacting with an AFM-ordered Fe dimer (gray balls with spins in arrows).

as linear bands and Fe d orbitals (the second term) are simplified as flatbands. The magnetic ordering was treated by assigning opposite spins for neighboring Fe atoms. The band structure was then obtained by direct diagonalization of the tight-binding Hamiltonian. We observe the energy gap for a single atomic Fe defect [Fig. 4(f)] but no gap for AFM-ordered Fe impurities [Fig. 4(g)], which is consistent with first-principles calculations. TSS may not distinguish a spin-degenerate single impurity from an AFM-ordered dimer [Fig. 4(h)]. In other words, the model Hamiltonian with magnetic impurities in AFM ordering is equivalent to the case of spin-degenerated impurities. Our calculations suggest that the decrease in TSS energy gap for high Fe concentrations in experiment [15] is similar to the case of AFM-ordered dimers. This picture will break down when the Fe distance in the dimers is increased. TSS may see individual Fe atoms in a dimer and experience the spin scattering to have a gap [Fig. 4(d)]. The spin-flipping scattering in TSS by magnetic impurities that favors AFM ordering may arise if $(\Delta k)^{-1}$ between TSS scattering states is comparable to the interatomic distance of magnetic impurities.

IV. SUMMARY

We investigated the magnetic phase transition and topological nature of surface states in Fe-doped Bi_2Se_3. The AFM phase is stable for the pristine case, regardless of Fe doping levels, but once the Fermi level is shifted up to lie in the conduction bands by intrinsic doping, the FM phase can be stabilized at dilute Fe doping levels (<1.7 at. %). At this regime, the FM phase is mediated by the conduction bands that have the same orbital character as the valence bands due to the band inversion of the topological insulating property. Above the critical concentration of ~1.7 at. %, localized spin states are coupled by the superexchange interaction and spins are aligned antiparallel to each other. We also found that Fe impurities tend to aggregate to form AFM-ordered clusters that serve as spin-degenerate impurities. As a result, TSS persists without the loss of topological insulating characteristics of the linear band dispersion and in-plane spin texture, even in the presence of Fe impurities. Our results suggest a possibility to control the electronic structure and magnetic phase of topological insulating materials by the transition-metal doping.

ACKNOWLEDGMENTS

This work was supported by the National Research Foundation of Korea through SRC program (Contract No. 2011-0030046) and the Supercomputing Center, Korea Institute of Science and Technology Information with supercomputing resources including technical support (Contract No. KSC-2013-C3-042).

[1] C. L. Kane and E. J. Mele, Phys. Rev. Lett. **95**, 146802 (2005).
[2] C. L. Kane and E. J. Mele, Phys. Rev. Lett. **95**, 226801 (2005).
[3] B. A. Bernevig, T. L. Hughes, and S.-C. Zhang, Science **314**, 1757 (2006).

[4] M. Konig, S. Wiedmann, C. Brune, A. Roth, H. Buhmann, L. W. Molenkamp, X.-L. Qi, and S.-C. Zhang, Science **318**, 766 (2007).
[5] D. Hsieh, D. Qian, L. Wray, Y. Xia, Y. S. Hor, R. J. Cava, and M. Z. Hasan, Nature (London) **452**, 970 (2008).
[6] Z. Alpichshev, J. G. Analytis, J. H. Chu, I. R. Fisher, Y. L. Chen, Z. X. Shen, A. Fang, and A. Kapitulnik, Phys. Rev. Lett. **104**, 016401 (2010).
[7] L. Fu and C. L. Kane, Phys. Rev. Lett. **100**, 096407 (2008).
[8] X.-L. Qi and S.-C. Zhang, Rev. Mod. Phys. **83**, 1057 (2011).
[9] I. Garate and M. Franz, Phys. Rev. Lett. **104**, 146802 (2010).
[10] R. Yu, W. Zhang, H.-J. Zhang, S.-C. Zhang, X. Dai, and Z. Fang, Science **329**, 61 (2010).
[11] C.-Z. Chang, J. Zhang, X. Feng, J. Shen, Z. Zhang, M. Guo, K. Li, Y. Ou, P. Wei, L.-L. Wang, Z.-Q. Ji, Y. Feng, S. Ji, X. Chen, J. Jia, X. Dai, Z. Fang, S.-C. Zhang, K. He, Y. Wang, L. Lu, X.-C. Ma, and Q.-K. Xue, Science **340**, 167 (2013).
[12] T. Schlenk, M. Bianchi, M. Koleini, A. Eich, O. Pietzsch, T. O. Wehling, T. Frauenheim, A. Balatsky, J. L. Mi, B. B. Iversen, J. Wiebe, A. A. Khajetoorians, P. Hofmann, and R. Wiesendanger, Phys. Rev. Lett. **110**, 126804 (2013).
[13] M. R. Scholz, J. Sánchez-Barriga, D. Marchenko, A. Varykhalov, A. Volykhov, L. V. Yashina, and O. Rader, Phys. Rev. Lett. **108**, 256810 (2012).
[14] Y. L. Chen, J.-H. Chu, J. G. Analytis, Z. K. Liu, K. Igarashi, H.-H. Kuo, X. L. Qi, S. K. Mo, R. G. Moore, D. H. Lu, M. Hashimoto, T. Sasagawa, S. C. Zhang, I. R. Fisher, Z. Hussain, and Z. X. Shen, Science **329**, 659 (2010).
[15] H.-J. Kim, K.-S. Kim, J.-F. Wang, V. A. Kulbachinskii, K. Ogawa, M. Sasaki, A. Ohnishi, M. Kitaura, Y.-Y. Wu, L. Li, I. Yamamoto, J. Azuma, M. Kamada, and V. Dobrosavljević, Phys. Rev. Lett. **110**, 136601 (2013).
[16] M. L. Cohen, Phys. Scr., T **1**, 5 (1982).
[17] G. Kresse and J. Hafner, Phys. Rev. B **47**, 558 (1993).
[18] J. P. Perdew, K. Burke, and M. Ernzerhof, Phys. Rev. Lett. **77**, 3865 (1996).
[19] A. Tkatchenko and M. Scheffler, Phys. Rev. Lett. **102**, 073005 (2009).
[20] J.-M. Zhang, W. Zhu, Y. Zhang, D. Xiao, and Y. Yao, Phys. Rev. Lett. **109**, 266405 (2012).
[21] H. Zhang, C.-X. Liu, X.-L. Qi, X. Dai, Z. Fang, and S.-C. Zhang, Nat. Phys. **5**, 438 (2009).
[22] P. W. Anderson, Phys. Rev. **79**, 350 (1950).
[23] C.-Z. Chang, P. Tang, Y.-L. Wang, X. Feng, K. Li, Z. Zhang, Y. Wang, L.-L. Wang, X. Chen, C. Liu, W. Duan, K. He, X.-C. Ma, and Q.-K. Xue, Phys. Rev. Lett. **112**, 056801 (2014).
[24] D. West, Y. Y. Sun, H. Wang, J. Bang, and S. B. Zhang, Phys. Rev. B **86**, 121201 (2012).
[25] Y. S. Hor, A. Richardella, P. Roushan, Y. Xia, J. G. Checkelsky, A. Yazdani, M. Z. Hasan, N. P. Ong, and R. J. Cava, Phys. Rev. B **79**, 195208 (2009).
[26] K. Sato, L. Bergqvist, J. Kudrnovský, P. H. Dederichs, O. Eriksson, I. Turek, B. Sanyal, G. Bouzerar, H. Katayama-Yoshida, V. A. Dinh, T. Fukushima, H. Kizaki, and R. Zeller, Rev. Mod. Phys. **82**, 1633 (2010).
[27] H. Ohno, A. Shen, F. Matsukura, A. Oiwa, A. Endo, S. Katsumoto, and Y. Iye, Appl. Phys. Lett. **69**, 363 (1996).
[28] A. D. Becke and E. R. Johnson, J. Chem. Phys. **124**, 221101 (2006).
[29] F. Tran and P. Blaha, Phys. Rev. Lett. **102**, 226401 (2009).